Light-induced Dynamic Restructuring of Cu Active Sites on TiO_2 for Low-temperature H_2 Production from Methanol and Water

Shunqin Luo[1], Hui Song[1,2]*, Fumihiko Ichihara[1], Mitsutake Oshikiri[3], Wenning Lu[1,4], Dai-Ming Tang[1], Sijie Li[1], Yunxiang Li[5], Yifan Li[6], Philo Davin[1], Tetsuya Kako[7], Huiwen Lin[8]*, Jinhua Ye[1,2]*

1. International Center for Materials Nanoarchitectonics (WPI-MANA), National Institute for Materials Science (NIMS), 1-1 Namiki, Tsukuba, Ibaraki, 305-0044, Japan.
2. TJU-NIMS International Collaboration Laboratory, School of Material Science and Engineering, Tianjin University, Tianjin, 300072, P. R. China.
3. International Center for Materials Nanoarchitectonics (WPI-MANA), National Institute for Materials Science (NIMS), 3-13 Sakura, Tsukuba, Ibaraki, 305-0003, Japan.
4. State Key Laboratory of Nuclear Resources and Environment, East China University of Technology, Nanchang, 330013, P. R. China.
5. School of Chemistry, Chemical Engineering and Biotechnology, Nanyang Technological University, 62 Nanyang Drive, Singapore, 637459, Singapore.
6. Vacuum Interconnected Nanotech Workstation (Nano-X), Suzhou Institute of Nano-Tech and Nano-Bionics, Chinese Academy of Sciences, Suzhou, 215123, P. R. China.
7. Hydrogen Production Catalyst Materials Group, Research Center for Energy and Environmental Materials (GREEN), National Institute for Materials Science (NIMS), 1-1 Namiki, Tsukuba, Ibaraki, 305-0044, Japan.
8. School of Materials Science and Engineering, Southeast University, Nanjing, 211189, P. R. China.

E-mail: hui.song@tju.edu.cn; linh@seu.edu.cn; jinhua.ye@nims.go.jp.

Abstract

The structure and configuration of reaction centers, which dominantly govern the catalytic behaviors, often undergo dynamic transformations under reaction conditions, yet little is known about how to exploit these features to favor the catalytic functions. Here, we demonstrate a facile light activation strategy over a TiO_2-supported Cu catalyst to regulate the dynamic restructuring of Cu active sites

during low-temperature methanol steam reforming. Under illumination, the thermally deactivated Cu/TiO_2 undergoes the structural restoration from inoperative Cu_2O to the originally active metallic Cu caused by photo-excited charge carriers from TiO_2, thereby leading to substantially enhanced activity and stability. Given low intensity solar irradiation, the optimized Cu/TiO_2 displays a H_2 production rate of 1724.1 μmol g^{-1} min^{-1}, outperforming most of the conventional photocatalytic and thermocatalytic processes. Taking advantages of the strong light-matter-reactant interaction, we achieve *in-situ* manipulation of the Cu active sites, suggesting the feasibility for real-time functionalization of catalysts.

Introduction

Hydrogen (H_2) is of great significance as an alternative clean energy carrier and chemical building block.[1-4] Using a stable liquid (e.g., CH_3OH) in the process of reforming with H_2O results in the release of H_2 with a high storage density, and enables a safe storage and transportation of H_2.[5, 6] The state-of-the-art procedures for methanol steam reforming (MSR) using representative copper-based catalysts are generally conducted at relatively high reaction temperatures (250–350 °C), consuming a massive amount of energy input.[7, 8] Pioneering works have demonstrated the low-temperature H_2 production through aqueous-phase methanol reforming, yet noble-metal-catalysts and/or high reaction pressure are still required to fully activate both CH_3OH and H_2O molecules.[5, 9] Therefore, it becomes quite an essential and indispensable task to develop an innovative strategy that enables efficient H_2 production from MSR under facile condition over non-noble-metal catalysts.

Introducing light energy into the conventional thermocatalysis has emerged as a promising strategy to achieve a more rapid conversion by activating reactants with photo-induced charge carriers.[10-15] More encouragingly, a few recent advances exemplified that the light irradiation can influence the configuration of catalytic active sites, rendering a dynamic evolution of catalyst to tune the overall performance.[16, 17] Basically, restructuring of the catalyst surface in response to reaction environment, such as structural[18-22] and/or compositional evolution,[23-25] is of paramount importance, as it not only determines the structure-performance relationship, but also governs the underlying mechanisms over genuine active sites.[26-28] Linic and co-authors revealed a visible-light-induced photo-switching of the Cu valence state, in which the localized surface plasmon resonance (LSPR) of metallic Cu core reduced oxide shell formed *in-situ* on Cu, favoring the selective propylene epoxidation.[16] This

strong light-matter interaction is achieved using Cu nanoparticles (NPs) with an adequate diameter (~40 nm), together with a critical threshold irradiance to maximize the exploitation of LSPR energy. Downsizing Cu NPs leads to a more coordinatively unsaturated surface,[8, 29] and their interaction with adsorbates would be amplified due to their inherent thermal instability,[30] enabling a more pronounced catalytic behavior in MSR. However, this could ultimately weaken the LSPR absorption/metallic nature by severe surface poisoning/transformation, making the small Cu NPs more susceptible to deactivation.[31] It remains largely unknown how to *in-situ* revive these deactivated materials under operating conditions to produce functioning catalysts that deliver outstanding activity with long-term stability.

Here, we present a simple approach, which is enabled by taking the advantage of strong interaction between TiO_2 and ultraviolet (UV) light, to manipulate the dynamically compositional and structural changes of the Cu active site under operating MSR conditions, favoring the surface catalytic behavior of Cu/TiO_2 catalysts for low-temperature H_2 production. We observe a rapid thermal deactivation caused by the oxidative restructuring of actively metallic Cu into Cu_2O. Introducing UV light under operating conditions stimulates the inoperative catalysts by initiating structural restoration from Cu_2O (light off) to metallic Cu (light on), which in turn, producing functioning catalysts to favor long-term and efficient H_2 production. Advanced *in-situ* investigations combined with density functional theory (DFT)-based molecular dynamic simulations serve as a powerful platform to unravel the fundamental mechanism and critical role of UV light in facilitating the restructuring and valence/compositional control of Cu species occur along the path to catalytic function. We believe that the concept of light-induced structural transformation is an effective and competent supplement to conventional activation treatment, and will provide numerous new opportunities for constructing a robust and long-lived catalytic process by optimizing the dynamic nature of active sites under operating conditions.

Results and discussion

Effect of illumination on the MSR performance

To explore the effect of light irradiation, the steady-state catalytic activity of MSR on 5.8% Cu/TiO_2 reduced by H_2 (named as Cu/TiO_2-H_2 hereafter) at a reaction temperature of 170 °C was measured in dark condition, followed by irradiation of light with different wavelengths (see details in

experimental section). Without light irradiation, the initial H_2 production rate maximized at 153.5 μmol g^{-1} min^{-1} and progressively decreased to 9.8 μmol g^{-1} min^{-1} after 105 min reaction (Figure 1a), accompanied with the color of the catalyst changed from black (Cu/TiO_2-H_2) to yellow (deactivated state, named as Cu/TiO_2-D hereafter; inset in Figure 1a). This indicates a possible structure change of Cu, probably from metallic state to oxidative state. When introducing visible light ($420 < \lambda < 720$ nm, 458.1 mW cm^{-2}), the catalytic performance was not altered, and the color of catalyst was maintained in yellow. The critical role of Cu LSPR in activating the catalysts was also excluded by comparing the catalytic behavior under dark or exposing visible light from the beginning of the reaction (metallic Cu) (Supplementary Figure 4). Surprisingly, upon irradiation of UV light ($300 < \lambda < 420$ nm, 67.9 mW cm^{-2}), the catalytic activity was sharply increased to 202.5 μmol g^{-1} min^{-1}, and the color of catalyst was converted into black (photo-activated state, named as Cu/TiO_2-PA hereafter), signifying a distinctive role of UV light in initiating the structural restoration of Cu (Figure 1a). An apparent quantum efficiency (AQE) of 66.0% was observed upon the irradiation of monochromatic light ($\lambda = 365$ nm) at 170 °C. A slight decrease in catalytic performance after 4 h reaction could be attributed to the coke formation, and regeneration of spent sample (calcination in air at 350 °C followed by reducing in H_2 atmosphere) can recover their catalytic performance. Additionally, UV–visible light irradiation ($300 < \lambda < 720$ nm, 628.0 mW cm^{-2}) led to a similar dynamic change process, with a more pronounced enhancement in activity and long-term stability, revealing a cooperative effect of UV–visible light in improving catalytic performance (Figure 1a). The observed rate enhancement might primarily attribute to charge-carrier-mediated reactant activation, albeit with the potential contribution of photothermal heating. The dynamic photo-activation process is reversible and can sustain multiple successive cycles without noticeable decrease in performance (Figure 1b).

Similar photo-activation behavior can be observed at reaction temperatures between 150 and 210 °C (Figure 1c), and simply increase the reaction temperature up to 210 °C without light irradiation did not trigger the activation of catalysts, ruling out the potential role of photo-induced heating effect (Supplementary Note 1). Meanwhile, the H_2 production rates under UV–visible light irradiation ($300 < \lambda < 720$ nm, 628.0 mW cm^{-2}) were much higher than those under UV light irradiation ($300 < \lambda < 420$ nm, 67.9 mW cm^{-2}) at different temperatures. The apparent activation energy was decreased from 77.0 to 67.9 kJ mol^{-1} (Supplementary Figure 5), and a linear dependence of reaction rate on visible light intensity further verified the distinctive role of visible-light-induced hot-carriers beyond simple

photothermal heating (Supplementary Table 1 and Supplementary Figure 6). We note that the reversible oxidation/photo-activation process was only observed when using TiO_2 as the support (see Supplementary Table 2 for the chemical composition of catalysts), and Cu/TiO_2 exhibited higher catalytic performance compared with other conventional metal oxide support (Supplementary Figure 7). To further prove the advantage of Cu/TiO_2 catalysts, solar-driven MSR under low photon-flux (512.0 mW cm^{-2}, 300–800 nm) was conducted without additional thermal energy input (see Supplementary Figure 8 and 9). Upon solar light irradiation, a surface temperature of 170 °C was detected over 5.8% Cu/TiO_2 catalyst, which exhibited significantly superior catalytic performance (1724.1 μmol g^{-1} min^{-1}) compared to the representative $Cu/ZnO/Al_2O_3$ (CZA) (784.6 μmol g^{-1} min^{-1}) and other noble-metal-based catalysts (Pt, Pd, and Au: 389.8, 137.4, and 75.7 μmol g^{-1} min^{-1}, respectively) under same irradiation condition (Figure 1d), outperforming most of the conventional photocatalytic and thermocatalytic process under mild reaction conditions (Supplementary Table 3). Only a trace amount of undesirable CO was produced, and other organic products (e.g., CH_2O and HCOOH) were not observed, suggesting an excellent selectivity of Cu/TiO_2 catalyst for initiating MSR (Supplementary Table 4). We suppose that UV-light could excite TiO_2 support to generate photo-induced electrons, which serve to induce the reduction of Cu oxide to Cu metal, and the resulted metallic Cu could further absorb visible light via LSPR to promote MSR/H_2 production.[32, 33]

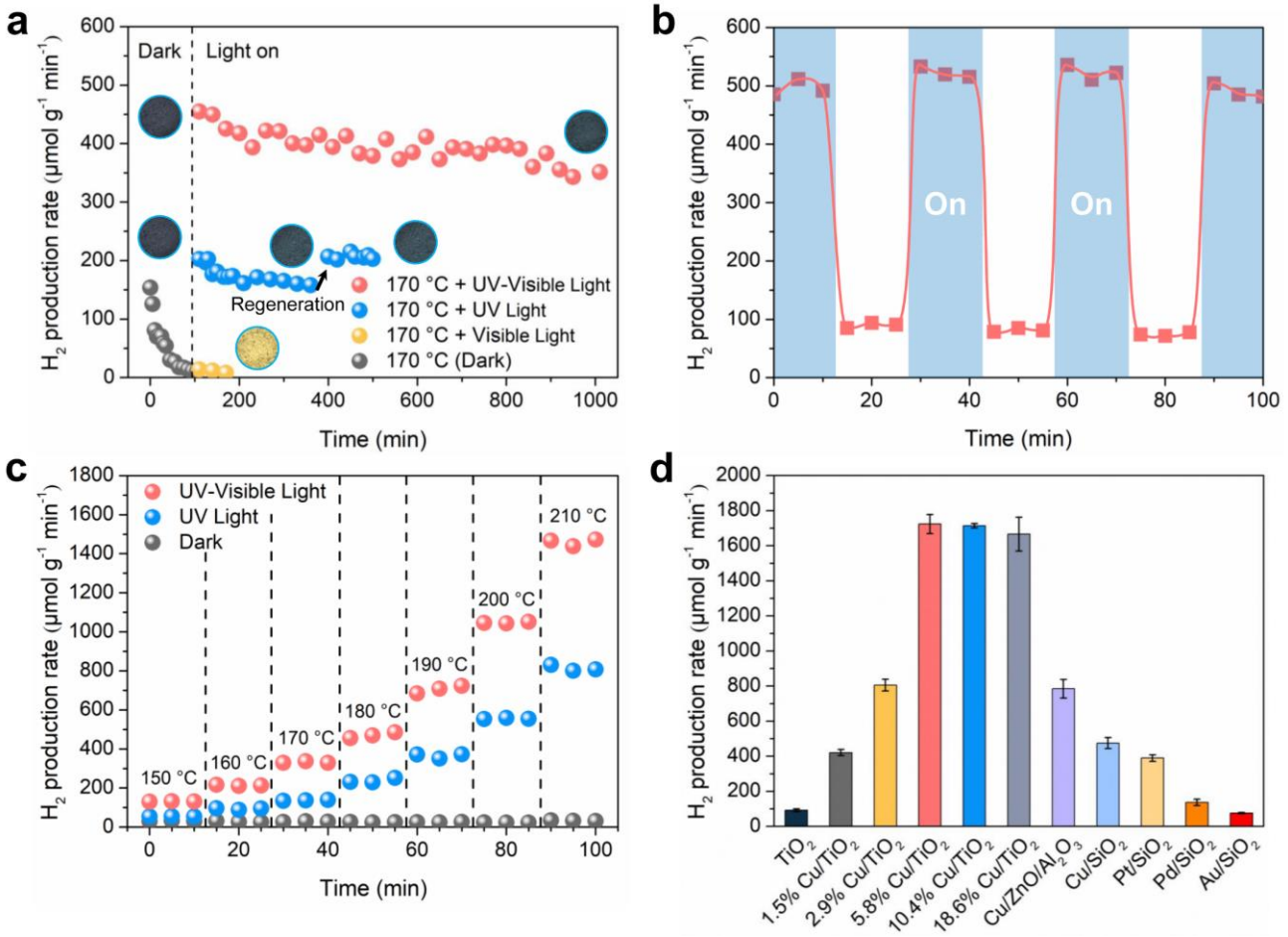

Figure 1. MSR activities of Cu/TiO_2 catalysts upon different light irradiation. **a**, Time-on-stream H_2 production over 5.8% Cu/TiO_2 under different light activation condition at 170 °C. Insets show representative photos of catalysts at different reaction stages, and the clear color change indicates possible configurational and valence changes occurred on catalysts during the reaction. **b**, Reversible photo-activation by UV–Vis light at 180 °C over 5.8% Cu/TiO_2. **c**, Light activation procedures under different reaction temperatures (150–210 °C) to validate the charge-carrier-initiated activation process. The catalysts were pre-deactivated under the thermocatalytic condition at 150 °C. **d**, Solar-driven MSR activity under the irradiation of low photon flux.

Structural change of Cu/TiO_2 in different reaction stages

The structures of catalysts were investigated to unravel the origin of their distinctive catalytic behavior. High-resolution transmission electron microscopy image (HR-TEM) of Cu/TiO_2-H_2 demonstrated a clear lattice fringe of 0.182 nm assigned to the (200) plane of metallic Cu (Figure 2a). Cu NPs with an average diameter of 3.0 nm were uniformly anchored on the surface of TiO_2 support

(Supplementary Figure 10), and a discrete distribution of Cu and TiO_2 was observed (Supplementary Figure 11). After the reaction in dark condition (Cu/TiO_2-D), a unique structural evolution of Cu was discerned. The surface atoms of Cu were deviated from their original position, leading to an obvious reconstruction of Cu NPs with a semi-coherent interface between TiO_2 support (Figure 2b). A lattice fringe of 0.210 nm in the reconstructed Cu NPs was demonstrated to be (200) plane of Cu_2O, and such an oxidation of Cu into Cu_2O was further confirmed by the high-resolution X-ray diffraction (XRD) patterns (Figure 2d). We propose that the reactant molecules trail the surface atoms of Cu NPs out of their original positions due to their strong interaction, as evidenced by the roughened surface of Cu NPs. Such a strong interaction resulted in the penetration of O atoms of reactants into the subsurface of Cu NPs during reaction. Notably, the oxidation of Cu NPs did not bring obvious sintering (Supplementary Figure 12 and 13). Due to the small size of Cu NPs that consist of only several lattice slabs, slight reconstruction of the atomic structure in surface/subsurface could induce the atomic re-arrangement of a whole nanoparticle. The atomic transformation of original active metallic Cu into oxides may enormously retard the surface catalytic reactions in respect of hindering the adsorption and bond activation of reactants.

With the assistance of photo-induced electrons from TiO_2 upon UV light excitation, the Cu_2O in Cu/TiO_2-D can readily revert to the activated state (photo-activated state, Cu/TiO_2-PA). The lattice fringe of Cu in Cu/TiO_2-PA was measured to be 0.203 nm, corresponding to the (111) plane of metallic Cu, whereas the semi-coherent interface between Cu and TiO_2 was preserved (Figure 2c). The reverted reconstruction of Cu active sites was also confirmed by high-resolution XRD (Figure 2d). Such a photo-activated reconstruction retarded the surface poisoning of Cu by maintaining the Cu NPs in the metallic state, thus rendering a promoted activity and stability upon light irradiation.

The chemical state change with dynamic restructuring was investigated through the Cu K-edge X-ray absorption near edge structure (XANES) spectra. The XANES spectrum over Cu/TiO_2-H_2 exhibited a similar absorption edge and shape of Cu foil, indicating the Cu species in Cu/TiO_2-H_2 were mainly in the metallic state (Figure 2e). Notably, upon the interaction with reactants in dark condition, the absorption edge of Cu in Cu/TiO_2-D distinctively shifted to higher energy, which is close to that of Cu^1 in Cu_2O reference. The XANES spectrum of Cu/TiO_2-PA displayed a similar feature to that of Cu/TiO_2-H_2, further validating the reduction of Cu^1 into Cu upon light irradiation (Figure 2e). Furthermore, the extended X-ray absorption fine structure (EXAFS) oscillations in *R* space (Figure 2f)

revealed that the Cu in Cu/TiO_2-H_2 and Cu/TiO_2-PA exhibited main characteristic features for the Cu−Cu bonds, whereas Cu/TiO_2-D showed no feature for the Cu−Cu with the appearance of Cu−O bonds. Specific characteristics of the Cu−Cu and Cu−O bonds can be obtained by fitting the EXAFS oscillation (Supplementary Figure 14–19 and Supplementary Table 5). The wavelet transforms contour plots of Cu/TiO_2-H_2 and Cu/TiO_2-PA displayed a maximum intensity at approximately 6–8 $Å^{-1}$, matching the Cu−Cu bond of Cu foil (Supplementary Figure 20). Comparatively, the maximum of the wavelet transform plot of Cu/TiO_2-D was located at 4–6 $Å^{-1}$, corresponding to the oxygen atoms surrounding the central copper atom.

All the above characterization results suggest that Cu active sites in Cu/TiO_2 experienced severe restructuring under operating MSR conditions, in which a full transformation of metallic Cu into Cu_2O under dark condition was observed. The strong interaction between Cu/TiO_2 and UV light, which is manifested by photo-excited charge carriers from TiO_2 support, activates the inoperative catalysts *in-situ*, rendering a dynamic transformation of Cu_2O back into catalytically active metallic Cu for a more facile surface reaction.

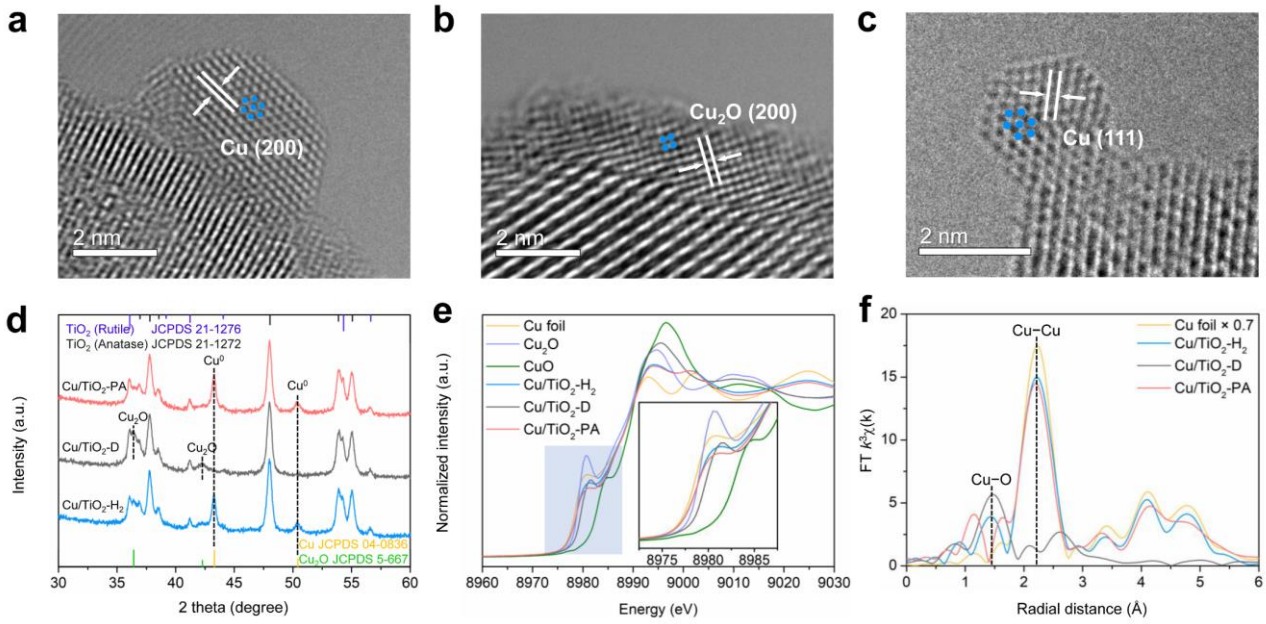

Figure 2. Structures of Cu/TiO_2 catalysts in different reaction stages. **a**, HR-TEM image of Cu/TiO_2-H_2. **b**, HR-TEM image of Cu/TiO_2-D. **c**, HR-TEM image of Cu/TiO_2-PA. **d**, XRD patterns of Cu/TiO_2 catalysts in different reaction stages. **e**, XANES spectra at Cu K-edge of Cu/TiO_2 catalysts in different states and reference samples. **f**, Fourier transformed Cu K-edge EXAFS oscillation of Cu/TiO_2 catalysts in different states and Cu foil.

In-situ investigation of dynamic restructuring on Cu/TiO_2

In-situ techniques provide more real-time evidences for a deeper understanding, although the above *ex-situ* characterizations confirmed the structural change of Cu active sites. Operando ultraviolet–visible diffuse reflectance spectra (UV–Vis DRS) of catalysts were investigated using a UV–Vis spectrophotometer equipped with an *in-situ* reaction cell. As presented in Figure 3a, the fresh sample (dark 1 min) demonstrated a typical LSPR absorption peak of metallic Cu at approximately 590 nm.[34, 35] Slight change of the surface oxidation condition of Cu species renders substantial shift of light absorption spectrum, which can be attributed to the fact that Cu LSPR is highly sensitive to local chemical state.[16, 35] After exposure of Cu/TiO_2 to MSR condition at 170 °C, the LSPR peak of Cu gradually disappeared with the appearance of a shoulder peak at an absorption edge of approximately 550 nm, which can be attributed to the transformation of Cu to Cu_2O, in accordance with observed color change during activity measurement. During the diminishing process of the Cu LSPR peak (590 nm), a gradual red-shift can be observed (inset in Figure 3a), suggesting that Cu NPs with smaller diameters were easier to be oxidized. Successive irradiation by UV light (67.9 mW cm^{-2}) induces a drastic transformation of chemical status of catalysts, manifested as the reduction of Cu_2O back into metallic Cu (reappearance of LSPR absorption peak at 590 nm). Similar light-activation process could not be initiated by using visible light solely, even the light intensity was as high as 458.1 mW cm^{-2} (Supplementary Figure 21), emphasizing the pivotal role of UV light in facilitating the valence and configuration change of Cu species (Supplementary Figure 22).

The oxidation state of Cu species was further monitored by *in-situ* diffuse reflectance infrared Fourier transform spectroscopy using CO as probe molecules (*in-situ* CO DRIFTS, see Supplementary Figure 23 and Supplementary Note 2 for peak assignment). In Cu/TiO_2-H_2, the Cu species were mostly in metallic states, as evidenced by the appearance of peaks at 2055 and 2105 cm^{-1} (Figure 3b). Compared to Cu/TiO_2-H_2, the signal intensity of CO adsorption in Cu/TiO_2-D (2105 cm^{-1}) was drastically diminished, which could be attributed to the substantial coverage of Cu species by surface reactants, lowering the adsorption capacity. The vanished peak at 2055 cm^{-1} (small metallic Cu NPs) and preserved absorption peak at 2173 cm^{-1} ($Cu^1(CO)_2$) in Cu/TiO_2-D concertedly verified the transformation of Cu into Cu^1 in Cu/TiO_2-D. Subsequent light activation led to the reduction of Cu^1 back into the metallic state, as can be observed by the increase of the bands in 2105 cm^{-1} with the re-

appearance of the small Cu NPs signal (2055 cm^{-1}) (Figure 3b). Such a chemical state evolution of Cu was further confirmed using *in-situ* near ambient pressure X-ray photoelectron spectroscopy (*in-situ* NAP XPS). As revealed by Cu 2p spectra (Figure 3c), Cu/TiO_2-H_2 only displayed Cu^0 feature, whereas a noticeable satellite peak (947.0 eV) corresponding to the Cu^1 feature was detected over Cu/TiO_2-D.[36] After introducing light, the Cu 2p spectrum changed back into a metallic Cu feature (Figure 3c). Combined with various *in-situ* techniques (UV–Vis DRS, CO DRIFTS and NAP XPS), the dynamic change of the oxidation state of Cu species in different reaction conditions was comprehensively revealed.

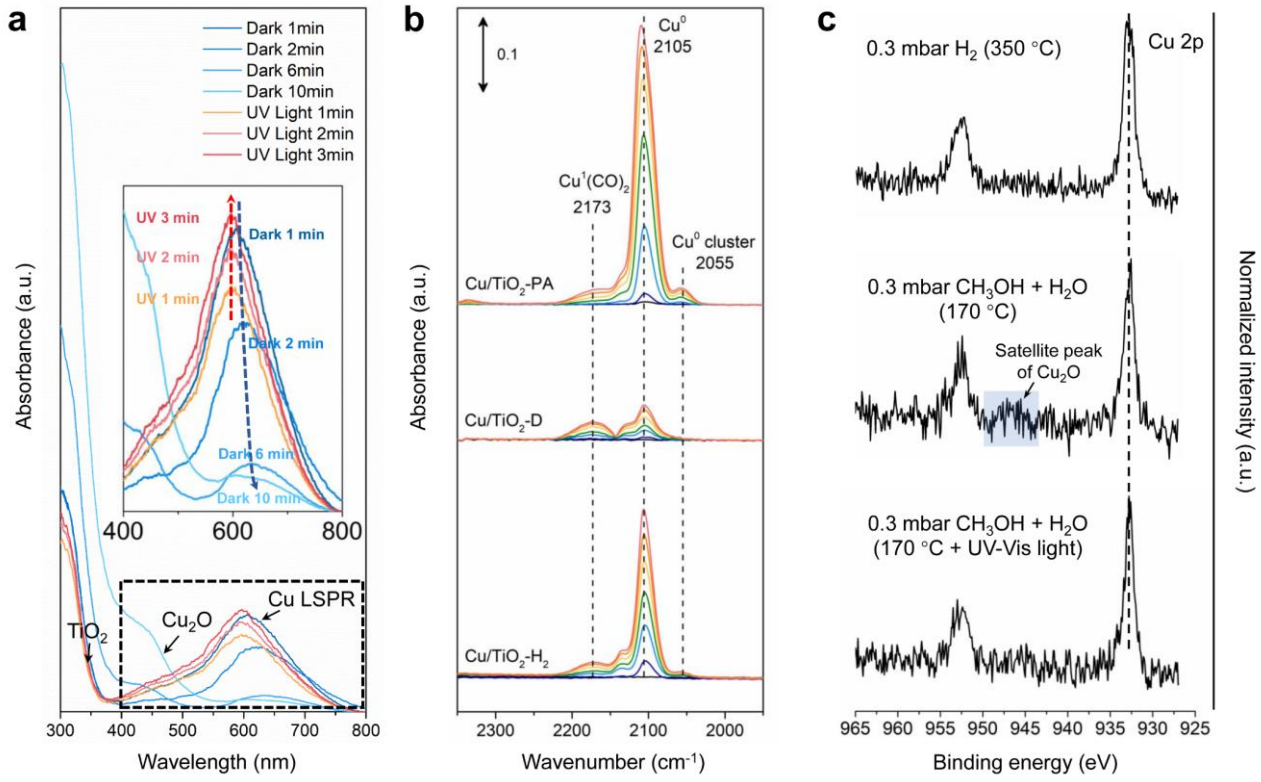

Figure 3. *In-situ* investigations of light-induced dynamic restructuring. **a**, *In-situ* UV–Vis absorption spectra of Cu/TiO_2 under different reaction conditions. **b**, *In-situ* CO DRIFTS spectra of the Cu/TiO_2 catalysts in different reaction stages. **c**, Cu 2p spectra of *in-situ* NAP XPS characterization under different reaction conditions, corresponding to Cu/TiO_2-H_2, Cu/TiO_2-D, and Cu/TiO_2-PA, respectively.

Correlation between the reaction intermediates and the dynamic restructuring

In-situ DRIFTS and *in-situ* NAP XPS were further applied to advance the understanding of the underlying mechanism for the observed oxidation and photo-induced activation of Cu. *In-situ* DRIFTS

analysis was conducted during MSR under dark or light conditions in order to provide further fundamental insights into how the light-matter interaction could facilitate a more efficient surface transformation. The reaction pathways for MSR have been well established according to previous literature,[37, 38] with the key intermediates involving $HCOOCH_3$, CH_2O, HCOOH, or CO identified over Cu-based catalysts (Supplementary Figure 24).[8, 39, 40] During measurement, no peaks related to gaseous or adsorbed CO (2100 to 2000 cm^{-1}) were observed in each reaction conditions, excluding the formation of CO as reaction intermediate.[41] The characteristic peaks at around 2360 cm^{-1} were defined as CO_2 (one of the products) (Figure 4a). Interestingly, under dark condition, the peak intensity increment of CO_2 gradually decreased, which could be attributed to the deactivation of catalysts at 170 °C under dark condition. Adding light energy can facilitate the reaction, as evidenced from the slope change, under light irradiation, peak intensity of CO_2 grew faster compared with that under dark condition (Figure 4b), which is in consistent with observed results in kinetic measurement. Under dark condition, C−H stretching vibrational modes of methanol species (around 2950 cm^{-1}) showed a slight decrease, followed by a sharp decrease after adding light, signifying a more pronounced conversion of methanol species upon light irradiation (Figure 4a).[42, 43] Furthermore, Cu−OCH_3 (1450 cm^{-1}) gradually became evident under dark condition, while it was disappeared after introducing light energy (Figure 4a).[23, 44] These phenomena indicate a severe accumulation of *CH_3O that bonds with Cu, which may block the Cu active site under dark condition. More importantly, the light can endow a more reactive surface by stimulating the decomposition of accumulated *CH_3O species for triggering succeeding conversion. As the result, after light irradiation, another upward peak related to the vibrational modes of *HCOO appeared at 1560 cm^{-1}, which was produced from successive conversion of the *CH_3O species (Figure 4a and b).[39]

To further probe the difference in residual adsorbates after reaction under dark or light condition, additional DRIFTS measurements were undertaken (Figure 4c). The background spectrum was firstly recorded in Ar atmosphere at 170 °C, followed by reaction with/without light irradiation for 30 min. Afterward, the chamber was purged by Ar gas for another 30 min to eliminate the weakly adsorbed species. Surface *CH_3O species (2937 and 2838 cm^{-1})[22, 44] and *HCOO species (1560 and 1361 cm^{-1})[22, 45] were identified under both dark and light condition. Compared to the residual species under dark condition, the surface coverage of *CH_3O species was decreased obviously under light condition. In contrast, a notable increase of *HCOO species can be observed under light condition, further verifying

the transformation of *CH_3O to *HCOO. Such a correlation indicates that the accumulation of *CH_3O might be the reason for the deactivation in dark condition, and more critically, with the assistance of light energy, *CH_3O species could be smoothly decomposed, rendering a swift turnover of consecutive reaction steps.

Long-lived surface adsorbates were further confirmed by C 1s spectra of *in-situ* NAP XPS measurements. C 1s spectrum in the fresh sample (0.3 mbar H_2, 350 °C) showed peaks at 285.0 and 286.0 eV from adventitious carbon (Figure 4d). After introducing gaseous reactants (0.3 mbar gaseous CH_3OH and H_2O, 170 °C), three external peaks centered at 288.1, 287.3, and 285.7 eV were observed, which correlate to gaseous CH_3OH, *HCOO, and *CH_3O−Cu species,[46-49] respectively, manifesting a substantial coverage of these predominant intermediates (Figure 4d). With the existence of these strongly bonded adsorbates, the Cu species could be gradually oxidized, whereas the chemical state of Ti and O remained nearly unchanged (Supplementary Figure 25). After introducing light, the surface coverage of the prominent intermediate (*CH_3O−Cu) was decreased (Figure 4d), accompanied with the Cu 2p spectrum changed back into metallic Cu feature (Figure 3c). The change behavior of Cu 2p and C 1s in the *in-situ* NAP XPS reveals the interrelation between the intermediate evolution and the dynamic change of the oxidation state of Cu species. Under dark condition, reaction intermediates are stable and strongly bond to Cu species, blocking the active site of Cu. More importantly, UV–visible light facilitates the decomposition and conversion of such long-lived adsorbates, which enables a dynamic change of Cu chemical state to facilitate surface catalytic transformations.

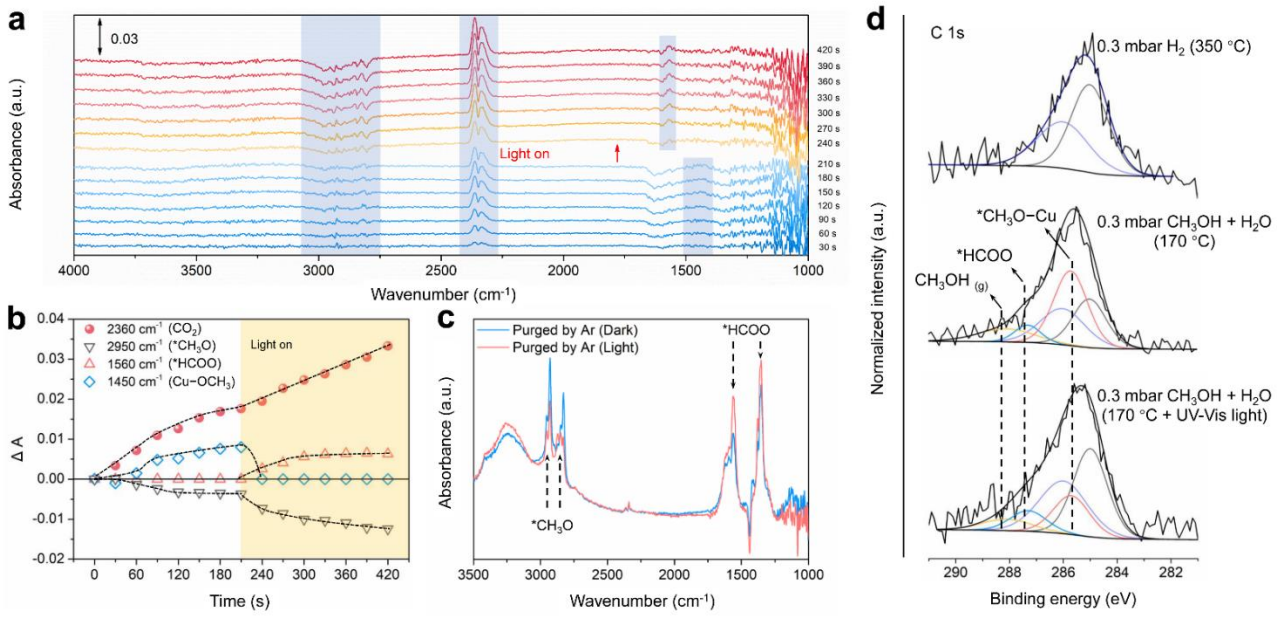

Figure 4. Correlations between the reaction intermediates and the dynamic restructuring. **a**, *In-situ* DRIFTS spectra of Cu/TiO_2 under dark and light conditions at reaction temperature of 170 °C. **b**, Slope change of the peak intensity of key intermediates derived from Figure 4a. **c**, Residual surface adsorbates after MSR with/without light irradiation. **d**, C 1s spectra in the *in-situ* NAP XPS characterization under different reaction conditions, corresponding to Cu/TiO_2-H_2, Cu/TiO_2-D, and Cu/TiO_2-PA, respectively.

First-principles molecular dynamics simulations

Two computational models (model A: Cu/TiO_2, and model B: Cu_2O/TiO_2, see Supplementary for detailed information) were constructed to simulate the motion of atoms (with molecules) and the corresponding electronic structure of the entire system using first-principles methods based on local-density approximations of density functional theory (DFT-LDA). First-principles quantum molecular dynamics simulations based on the Car-Parrinello method (CPMD) were used to investigate the state of each model in thermal equilibrium at 170 °C.

In model A (Cu/TiO_2), spontaneous dissociative adsorption of CH_3OH can be observed, forming $*CH_3O$ species near the interface between Cu and TiO_2 (Supplementary Figure 26). The accumulation of such species is supposed to be responsible for the observed oxidation of Cu due to the strong metal-reactant interaction. Since the electronic structure of Cu metals was superimposed on TiO_2, metallic Cu is proposed to serve as a charge transfer channel, delivering UV-excited electrons from TiO_2 to reactants (See supplementary Note 3 for detailed discussion).

In model B (Cu_2O/TiO_2), spontaneously dissociative adsorption of CH_3OH resulted in two sets of species. One was $(-Ti)-OCH_3$ and $(-Cu-O)-H$ in the interface between Cu_2O and TiO_2 (Figure 5a), and another was $(-Ti)-OCH_3$ and $(-Ti-O)-H$ on the TiO_2 surface (Figure 5b). At this moment, the electronic structure of Cu_2O was found to be superimposed on the electronic structure of TiO_2 formed by Ti 3d and O 2p (Figure 5c). The upper edge of the Cu 3d band was well mixed with the lower edge of Ti 3d band and O 2p band of Cu_2O, whereas the density of state in O 2p band of TiO_2 near this energy was much smaller than that of O 2p band of Cu_2O (marked in red in Figure 5c). In this case, the UV-excited electrons of O 2p of TiO_2 could enter the Ti 3d band and simultaneously inject into the Cu 3d band with the additional help of the O 2p wavefunction of Cu_2O, reducing the formed Cu_2O into metallic Cu. As the result, photo-induced electrons from the TiO_2 were mostly consumed in the

reduction of Cu_2O due to the strong wavefunction coupling between Cu_2O and TiO_2. Looking at the O 2p components of (−Ti)−OH and (−Ti)−OCH_3 formed by dissociative adsorption of H_2O and CH_3OH, releasing H from −OH or from that of −OCH_3 can be expected by inducing unstable states due to the electron extraction upon UV irradiation (Supplementary Figure 27).

Our simulations demonstrate the role of photo-induced charge carriers and *CH_3O species during dynamic restructuring of Cu. The accumulation of *CH_3O species, produced from CH_3OH activation via TiO_2 (see Supplementary Note 4 and reference[50]), plays a decisive role in inducing the oxidative restructuring of Cu to Cu_2O. Once the light is applied, the UV-excited electrons from TiO_2 could initiate reductive structuring of as-oxidized Cu_2O into metallic Cu with the assistance of O 2p wavefunction of Cu_2O, resulting in a dynamical restructuring of Cu (Figure 5d). Consequently, due to the plasmonic nature of metallic Cu, visible light can be utilized to produce hot carriers, which could cooperate with the charge carriers from TiO_2 to further promote the surface reaction. Such a cooperative photoactivation process, together with resulting structural optimization, concertedly contribute to the outstanding performance of dynamic photocatalysis.

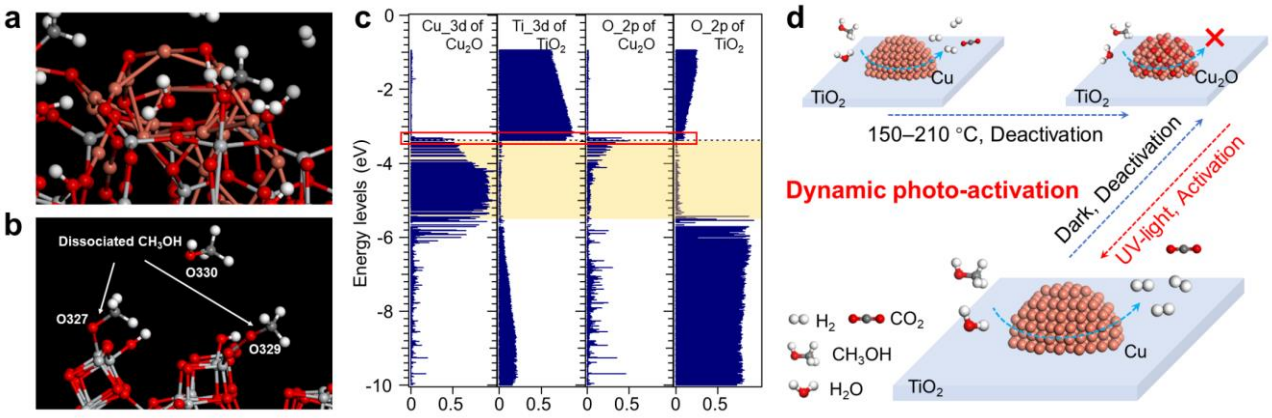

Figure 5. DFT-based first-principles molecular dynamics simulation and proposed process for photo-initiated dynamic structural evolution on Cu/TiO_2 catalysts. **a,** Geometry at the moment when the CH_3OH came close to the interface between Cu_2O and TiO_2 support. **b,** Geometry at the moment of dissociative adsorption of CH_3OH on TiO_2 surface. **c**, Electronic properties of model B (Cu_2O/TiO_2) thermally equilibrated at 443 K. Gray, brown, red, dark gray and white indicate Ti, Cu, O, C, and H, respectively. Black broken line indicates the highest occupied level, and yellow shadow indicates the band gap of TiO_2 support. **d**, Schematic illustration of dynamic reversible photo-activation process.

Conclusion

We demonstrate a solar-induced dynamic restructuring over Cu/TiO_2 catalysts to revive the catalytic activity for low-temperature H_2 production. Specifically, Cu nanoparticles undergo an oxidative restructuring into Cu_2O with severe thermal deactivation under the dark condition, while it manifests a sharp increase in catalytic activity and stability due to the UV light-induced reductive restoration into metallic Cu. *In-situ* characterizations combined with DFT-based molecular dynamics provide a comprehensive insight into how the light-matter-reactant interaction drives the structural and chemical change of Cu. The accumulated adsorbates of $*CH_3O$ under dark condition oxidize the Cu active sites, whereas the UV-excited electrons from TiO_2 facilitate Cu restructuring to promote the adsorbate dissociation. Besides, the reverted plasmonic Cu could capture visible light to further promote the surface reaction. The interplay of UV and visible light renders a cooperative photo-activation process, enhancing the stability with activity outperforming most of the conventional photocatalytic and thermocatalytic processes. This study demonstrates a novel and feasible strategy to regulate the structural evolution of active surface sites during the reaction, which in turn provides alternative protocols to construct a highly efficient and stable reaction center toward broader and more sustainable industrial reactions.

Acknowledgements

This work was financially supported by JSPS KAKENHI (JP18H02065, JP21K04782), the World Premier International Research Center Initiative (WPI Initiative) on Materials Nanoarchitectonics (MANA), MEXT (Japan), Photoexcitonix Project in Hokkaido University, National Natural Science Foundation of China (Grant No. 42103016). The first principles calculations in this study were performed on the Numerical Materials Simulator at NIMS. TEM characterization was supported by NIMS Electron Microscopy Analysis Station, Nanostructural Characterization Group.

Associated Content

Supporting Information

The Supporting Information is available free of charge

The detail experimental procedures, supplementary discussions, ICP-OES data, activity comparison, DFT calculation.

Notes

The authors declare that they have no competing interests.

References

1. Yuan, Y.; Zhou, L.; Robatjazi, H.; Bao, J. L.; Zhou, J.; Bayles, A.; Yuan, L.; Lou, M.; Lou, M.; Khatiwada, S.; Carter, E. A.; Nordlander, P.; Halas, N. J., Earth-abundant photocatalyst for H_2 generation from NH_3 with light-emitting diode illumination. *Science* **2022,** *378* (6622), 889-893.
2. Jacobson, M. Z.; Colella, W.; Golden, D., Cleaning the air and improving health with hydrogen fuel-cell vehicles. *Science* **2005,** *308* (5730), 1901-1905.
3. Cohen, R. L.; Wernick, J., Hydrogen storage materials: properties and possibilities. *Science* **1981,** *214* (4525), 1081-1087.
4. Song, H.; Luo, S.; Huang, H.; Deng, B.; Ye, J., Solar-driven hydrogen production: recent advances, challenges, and future perspectives. *ACS Energy Lett.* **2022,** *7* (3), 1043-1065.
5. Lin, L.; Yu, Q.; Peng, M.; Li, A.; Yao, S.; Tian, S.; Liu, X.; Li, A.; Jiang, Z.; Gao, R.; Han, X.; Li, Y.-w.; Wen, X.-d.; Zhou, W.; Ma, D., Atomically dispersed Ni/α-MoC catalyst for hydrogen production from methanol/water. *J. Am. Chem. Soc.* **2021,** *143* (1), 309-317.
6. Chen, L.; Qi, Z.; Peng, X.; Chen, J.-L.; Pao, C.-W.; Zhang, X.; Dun, C.; Young, M.; Prendergast, D.; Urban, J. J.; Guo, J.; Somorjai, G. A.; Su, J., Insights into the mechanism of methanol steam reforming tandem reaction over CeO_2 supported single-site catalysts. *J. Am. Chem. Soc.* **2021,** *143* (31), 12074-12081.
7. Palo, D. R.; Dagle, R. A.; Holladay, J. D., Methanol steam reforming for hydrogen production. *Chem. Rev.* **2007,** *107* (10), 3992-4021.
8. Sá, S.; Silva, H.; Brandão, L.; Sousa, J. M.; Mendes, A., Catalysts for methanol steam reforming—A review. *Appl. Catal., B* **2010,** *99* (1), 43-57.
9. Lin, L.; Zhou, W.; Gao, R.; Yao, S.; Zhang, X.; Xu, W.; Zheng, S.; Jiang, Z.; Yu, Q.; Li, Y.-W.; Shi, C.; Wen, X.-D.; Ma, D., Low-temperature hydrogen production from water and methanol using Pt/α-MoC catalysts. *Nature* **2017,** *544* (7648), 80-83.
10. Aslam, U.; Rao, V. G.; Chavez, S.; Linic, S., Catalytic conversion of solar to chemical energy on plasmonic metal nanostructures. *Nat. Catal.* **2018,** *1* (9), 656-665.
11. Linic, S.; Chavez, S.; Elias, R., Flow and extraction of energy and charge carriers in hybrid plasmonic nanostructures. *Nat. Mater.* **2021,** *20* (7), 916-924.
12. Brongersma, M. L.; Halas, N. J.; Nordlander, P., Plasmon-induced hot carrier science and technology. *Nat. Nanotechnol.* **2015,** *10* (1), 25-34.
13. L. Zhou; D. F. Swearer; C. Zhang; H. Robatjazi; H. Zhao; L. Henderson; L. Dong; P. Christopher; E. A. Carter; P. Nordlander; Halas, N. J., Quantifying hot carrier and thermal contributions in plasmonic photocatalysis. *Science* **2018,** *362* (6410), 69-72.
14. Lin, H.; Luo, S.; Zhang, H.; Ye, J., Toward solar-driven carbon recycling. *Joule* **2022,** *6* (2), 294-314.
15. Lv, C.; Bai, X.; Ning, S.; Song, C.; Guan, Q.; Liu, B.; Li, Y.; Ye, J., Nanostructured materials for photothermal carbon dioxide hydrogenation: regulating solar utilization and catalytic performance. *ACS Nano* **2023,** *17* (3), 1725-1738.
16. Marimuthu, A.; Zhang, J.; Linic, S., Tuning selectivity in propylene epoxidation by plasmon mediated photo-

switching of Cu oxidation state. *Science* **2013,** *339* (6127), 1590-1593.
17. Lee, B.-H.; Park, S.; Kim, M.; Sinha, A. K.; Lee, S. C.; Jung, E.; Chang, W. J.; Lee, K.-S.; Kim, J. H.; Cho, S.-P.; Kim, H.; Nam, K. T.; Hyeon, T., Reversible and cooperative photoactivation of single-atom Cu/TiO_2 photocatalysts. *Nat. Mater.* **2019,** *18* (6), 620-626.
18. Yang, J.; Qi, H.; Li, A.; Liu, X.; Yang, X.; Zhang, S.; Zhao, Q.; Jiang, Q.; Su, Y.; Zhang, L.; Li, J.-F.; Tian, Z.-Q.; Liu, W.; Wang, A.; Zhang, T., Potential-driven restructuring of Cu single atoms to nanoparticles for boosting the electrochemical reduction of nitrate to ammonia. *J. Am. Chem. Soc.* **2022,** *144* (27), 12062-12071.
19. Xing, G.; Tong, M.; Yu, P.; Wang, L.; Zhang, G.; Tian, C.; Fu, H., Reconstruction of highly dense Cu−N_4 active sites in electrocatalytic oxygen reduction characterized by operando synchrotron radiation. *Angew. Chem. Int. Ed* **2022,** *61* (40), e202211098.
20. Bai, X.; Zhao, X.; Zhang, Y.; Ling, C.; Zhou, Y.; Wang, J.; Liu, Y., Dynamic stability of copper single-atom catalysts under working conditions. *J. Am. Chem. Soc.* **2022,** *144* (37), 17140-17148.
21. Yuan, W.; Zhu, B.; Fang, K.; Li, X.-Y.; Hansen, T. W.; Ou, Y.; Yang, H.; Wagner, J. B.; Gao, Y.; Wang, Y.; Zhang, Z., In situ manipulation of the active Au-TiO_2 interface with atomic precision during CO oxidation. *Science* **2021,** *371* (6528), 517-521.
22. Li, D.; Xu, F.; Tang, X.; Dai, S.; Pu, T.; Liu, X.; Tian, P.; Xuan, F.; Xu, Z.; Wachs, I. E.; Zhu, M., Induced activation of the commercial Cu/ZnO/Al_2O_3 catalyst for the steam reforming of methanol. *Nat. Catal.* **2022,** *5* (2), 99-108.
23. Yang, H.; Chen, Y.; Cui, X.; Wang, G.; Cen, Y.; Deng, T.; Yan, W.; Gao, J.; Zhu, S.; Olsbye, U.; Wang, J.; Fan, W., A highly stable copper-based catalyst for clarifying the catalytic roles of Cu^0 and Cu^+ species in methanol dehydrogenation. *Angew. Chem. Int. Ed.* **2018,** *57* (7), 1836-1840.
24. Zugic, B.; Wang, L.; Heine, C.; Zakharov, D. N.; Lechner, B. A. J.; Stach, E. A.; Biener, J.; Salmeron, M.; Madix, R. J.; Friend, C. M., Dynamic restructuring drives catalytic activity on nanoporous gold–silver alloy catalysts. *Nat. Mater.* **2017,** *16* (5), 558-564.
25. Muravev, V.; Spezzati, G.; Su, Y.-Q.; Parastaev, A.; Chiang, F.-K.; Longo, A.; Escudero, C.; Kosinov, N.; Hensen, E. J. M., Interface dynamics of Pd–CeO_2 single-atom catalysts during CO oxidation. *Nat. Catal.* **2021,** *4* (6), 469-478.
26. Luo, L.; Nian, Y.; Wang, S.; Dong, Z.; He, Y.; Han, Y.; Wang, C., Real-time atomic-scale visualization of reversible copper surface activation during the CO oxidation reaction. *Angew. Chem. Int. Ed.* **2020,** *59* (6), 2505-2509.
27. Matsubu, J. C.; Zhang, S.; DeRita, L.; Marinkovic, N. S.; Chen, J. G.; Graham, G. W.; Pan, X.; Christopher, P., Adsorbate-mediated strong metal–support interactions in oxide-supported Rh catalysts. *Nat. Chem.* **2017,** *9* (2), 120-127.
28. Liu, L.; Corma, A., Structural transformations of solid electrocatalysts and photocatalysts. *Nat. Rev. Chem.* **2021,** *5* (4), 256-276.
29. Tong, W.; West, A.; Cheung, K.; Yu, K.-M.; Tsang, S. C. E., Dramatic effects of gallium promotion on methanol steam reforming Cu–ZnO catalyst for hydrogen production: formation of 5 Å copper clusters from Cu–$ZnGaO_x$. *ACS Catal.* **2013,** *3* (6), 1231-1244.
30. Christopher, P.; Xin, H.; Linic, S., Visible-light-enhanced catalytic oxidation reactions on plasmonic silver nanostructures. *Nat. Chem.* **2011,** *3* (6), 467-472.
31. Martín, A. J.; Mitchell, S.; Mondelli, C.; Jaydev, S.; Pérez-Ramírez, J., Unifying views on catalyst deactivation. *Nat. Catal.* **2022,** *5* (10), 854-866.
32. Christopher, P.; Xin, H.; Marimuthu, A.; Linic, S., Singular characteristics and unique chemical bond activation mechanisms of photocatalytic reactions on plasmonic nanostructures. *Nat. Mater.* **2012,** *11* (12), 1044-1050.
33. Luo, S.; Ren, X.; Lin, H.; Song, H.; Ye, J., Plasmonic photothermal catalysis for solar-to-fuel conversion: current status and prospects. *Chem. Sci.* **2021,** *12* (16), 5701-5719.

34. Linic, S.; Christopher, P.; Ingram, D. B., Plasmonic-metal nanostructures for efficient conversion of solar to chemical energy. *Nat. Mater.* **2011,** *10* (12), 911-21.
35. Linic, S.; Aslam, U.; Boerigter, C.; Morabito, M., Photochemical transformations on plasmonic metal nanoparticles. *Nat. Mater.* **2015,** *14* (6), 567-576.
36. Ghijsen, J.; Tjeng, L. H.; van Elp, J.; Eskes, H.; Westerink, J.; Sawatzky, G. A.; Czyzyk, M. T., Electronic structure of Cu_2O and CuO. *Phys. Rev. B* **1988,** *38* (16), 11322-11330.
37. Takahashi, K.; Takezawa, N.; Kobayashi, H., The mechanism of steam reforming of methanol over a copper-silica catalyst. *Appl. Catal.* **1982,** *2* (6), 363-366.
38. Takezawa, N.; Iwasa, N., Steam reforming and dehydrogenation of methanol: Difference in the catalytic functions of copper and group VIII metals. *Catal. Today* **1997,** *36* (1), 45-56.
39. Luo, S.; Lin, H.; Wang, Q.; Ren, X.; Hernández-Pinilla, D.; Nagao, T.; Xie, Y.; Yang, G.; Li, S.; Song, H.; Oshikiri, M.; Ye, J., Triggering water and methanol activation for solar-driven H_2 production: interplay of dual active sites over plasmonic ZnCu alloy. *J. Am. Chem. Soc.* **2021,** *143* (31), 12145-12153.
40. Santacesaria, E.; Carrá, S., Kinetics of catalytic steam reforming of methanol in a cstr reactor. *Appl. Catal.* **1983,** *5* (3), 345-358.
41. Weigel, J.; Koeppel, R. A.; Baiker, A.; Wokaun, A., Surface species in CO and CO_2 hydrogenation over copper/zirconia: on the methanol synthesis mechanism. *Langmuir* **1996,** *12* (22), 5319-5329.
42. Clarke, D. B.; Lee, D. K.; Sandoval, M. J.; Bell, A. T., Infrared studies of the mechanism of methanol decomposition on Cu/SiO_2. *J. Catal.* **1994,** *150* (1), 81-93.
43. Lochař, V., FT-IR study of methanol, formaldehyde and methyl formate adsorption on the surface of Mo/Sn oxide catalyst. *Appl. Catal., A* **2006,** *309* (1), 33-36.
44. Kaftan, A.; Kusche, M.; Laurin, M.; Wasserscheid, P.; Libuda, J., KOH-promoted Pt/Al_2O_3 catalysts for water gas shift and methanol steam reforming: an operando DRIFTS-MS study. *Appl. Catal., B* **2017,** *201*, 169-181.
45. Wang, Y.; Gao, W.; Li, K.; Zheng, Y.; Xie, Z.; Na, W.; Chen, J. G.; Wang, H., Strong evidence of the role of H_2O in affecting methanol selectivity from CO_2 hydrogenation over $Cu-ZnO-ZrO_2$. *Chem* **2020,** *6* (2), 419-430.
46. Favaro, M.; Xiao, H.; Cheng, T.; Goddard, W. A.; Yano, J.; Crumlin, E. J., Subsurface oxide plays a critical role in CO_2 activation by Cu(111) surfaces to form chemisorbed CO_2, the first step in reduction of CO_2. *Proc. Natl. Acad. Sci. U.S.A.* **2017,** *114* (26), 6706-6711.
47. Liu, Z.; Huang, E.; Orozco, I.; Liao, W.; Palomino, R. M.; Rui, N.; Duchoň, T.; Nemšák, S.; Grinter, D. C.; Mahapatra, M.; Liu, P.; Rodriguez, J. A.; Senanayake, S. D., Water-promoted interfacial pathways in methane oxidation to methanol on a CeO_2-Cu_2O catalyst. *Science* **2020,** *368* (6490), 513-517.
48. Zhang, Y.; Liu, G.; Shi, L.; Wu, P.; Zeng, G.; Zhang, C.; Yang, N.; Li, S.; Sun, Y., Quantitative conversion of methanol to methyl formate on graphene-confined nano-oxides. *iScience* **2020,** *23* (6), 101157.
49. Huang, E.; Orozco, I.; Ramírez, P. J.; Liu, Z.; Zhang, F.; Mahapatra, M.; Nemšák, S.; Senanayake, S. D.; Rodriguez, J. A.; Liu, P., Selective methane oxidation to methanol on $ZnO/Cu_2O/Cu(111)$ catalysts: multiple site-dependent behaviors. *J. Am. Chem. Soc.* **2021,** *143* (45), 19018-19032.
50. Oshikiri, M.; Boero, M.; Matsushita, A.; Ye, J., Water molecule adsorption properties on surfaces of MVO_4 (M = In, Y, Bi) photo-catalysts. *J. Electroceram.* **2009,** *22* (1), 114-119.

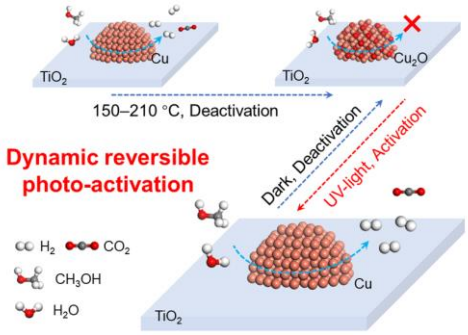
TiO2
Cu
TiO2
Cu2O
150–210 °C, Deactivation
Dark, Deactivation
UV-light, Activation
Dynamic reversible
photo-activation
H2
CO2
CH3OH
H2O
Cu
TiO2

TOC graphic